Multi-fragment partitions in the 32 to 95 AMeV ^{36}Ar+^{58}Ni reactions

J.L. Charvet, L. Nalpas, B. Borderie, R. Dayras, D. Dore, M.F. Rivet, M. Assenard, G. Auger, Ch.O. Bacri, J. Benlliure, et al.

CEA/SACLAY
DSM

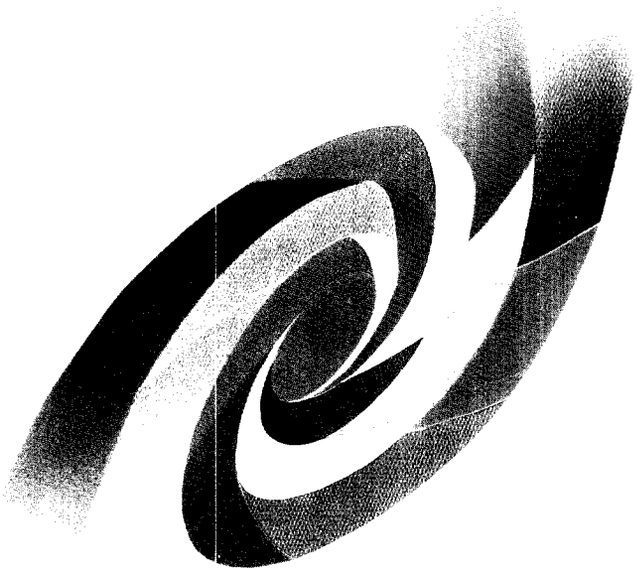

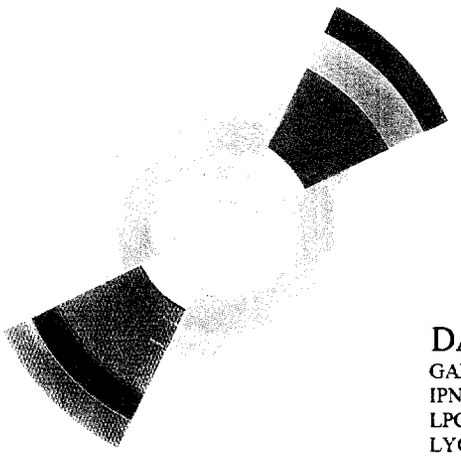

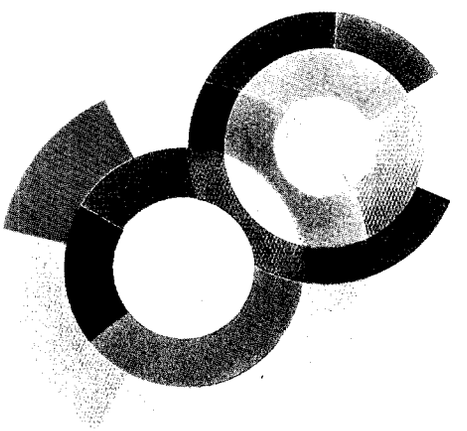

DAPNIA/SPhN-97-22 04/1997
GANIL P97-10
IPNO-DRE-97-13
LPCC 97-09
LYCEN 9712
SUBATECH 97-09

Multi-fragment partitions in the 32 to 95 AMeV ^{36}Ar + ^{58}Ni reactions

J.-L. Charvet, L. Nalpas, B. Borderie, R. Dayras, D. Doré, M.F. Rivet, M. Assenard, G. Auger, Ch.O. Bacri, J. Benlliure, E. Bisquer, R. Bougault, F. Bocage, R. Brou, P. Buchet, A. Chbihi, J. Colin, D. Cussol, E. De Filippo, A. Demeyer, D. Durand, P. Eudes, J.D. Frankland, E. Galichet, E. Genouin-Duhamel, E. Gerlic, M. Germain, D. Gourio, D. Guinet, P. Lautesse, J.L. Laville, J.F. Lecolley, A. Le Fèvre, T. Lefort, R. Legrain, O. Lopez, M. Louvel, N. Marie, V. Métivier, A.D. Nguyen, M. Parlog, J. Péter, E. Plagnol, A. Rahmani, T. Reposeur, E. Rosato, F. Saint-Laurent, S. Salou, M. Squalli, J.C. Steckmeyer, M. Stern, B. Tamain, O. Tirel, L. Tassan-Got, E. Vient, C. Volant, J.P. Wieleczko

DAPNIA

Département d'Astrophysique, de Physique des Particules, de Physique Nucléaire et de l'Instrumentation Associée
CEA/Saclay F-91191 Gif-sur-Yvette Cédex

XXXVth International Winter Meeting on
Nuclear Physics,
BORMIO, Italy, 3-8 February 1997

MULTI-FRAGMENT PARTITIONS IN THE 32 to 95 AMeV ^{36}Ar+^{58}Ni REACTIONS

J-L. Charvet[1], L. Nalpas[1], B. Borderie[2], R. Dayras[1], D. Doré[2], M.F. Rivet[2], M. Assenard[6], G. Auger[3], Ch.O. Bacri[2], J. Benlliure[3], E. Bisquer[5], R. Bougault[4], F. Bocage[4], R. Brou[4], P. Buchet[1], A. Chbihi[3], J. Colin[4], D. Cussol[4], E. De Filippo[1,3], A. Demeyer[5], D. Durand[4], P. Eudes[6], J.D. Frankland[2], E. Galichet[5], E. Genouin-Duhamel[4], E. Gerlic[5], M. Germain[6], D. Gourio[6], D. Guinet[5], P. Lautesse[5], J.L. Laville[6], J.F. Lecolley[4], A. Le Fèvre[3], T. Lefort[4], R. Legrain[1], O. Lopez[4], M. Louvel[4], N. Marie[3], V. Métivier[4], A.D. Nguyen[4], M. Parlog[7], J. Péter[4], E. Plagnol[2], A. Rahmani[6], T. Reposeur[6], E. Rosato[8], F. Saint-Laurent[3], S. Salou[3], M. Squalli[2], J.C. Steckmeyer[4], M. Stern[5], B. Tamain[4], O. Tirel[3], L. Tassan-Got[2], E. Vient[4], C. Volant[1], J.P. Wieleczko[3]

(1) CEA, DAPNIA/SPhN, CE Saclay, F-91191 Gif-sur-Yvette Cedex, France
(2) IPN, IN2P3-Université Paris Sud, F-91406 Orsay, France
(3) GANIL, B.P.5027 - 14021 Caen Cedex, France
(4) LPC, ISMRA, IN2P3-CNRS F-14050 Caen Cedex, France
(5) IPN Lyon, IN2P3-CNRS et Université, F-69622 Villeurbanne Cedex, France
(6) SUBATECH, IN2P3-CNRS et Université, F-44072 Nantes Cedex 03, France
(7) Institute of Physics and Nuclear Engineering, IFA, P.O. Box MG6, Bucharest, Romania
(8) Dipartimento di Scienze, Univ. di Napoli, 80125 Napoli, Italy

Abstract

Using the 4π multidetector array INDRA at GANIL, we have investigated the reaction ^{36}Ar+^{58}Ni for bombarding energies ranging from 32 to 95 AMeV. Over this energy domain, quasi-binary dissipative collisions are the dominant process exhausting more than 90% of the reaction cross-section. Nevertheless, at 32 AMeV incident energy, detection of residual nuclei seems to indicate that incomplete fusion is present. For binary collisions the excitation energy sharing between the quasi-projectile (QP) and the quasi-target (QT) is not thermalized suggesting a thermalization time longer than the interaction time. The study of the multi-fragment partitions shows clearly that the QP and the QT decay independently from one another.

I Introduction

The recent advent of 4π detection arrays with high geometrical efficiency, good granularity and low detection energy thresholds permits to investigate the properties of highly excited nuclei created in nucleus-nucleus collisions in the intermediate energy domain (20 MeV<E/A<100 MeV). At low excitation energy, nuclei usually disintegrate by emitting neutrons and light charged particles (Z=1,2), whereas at higher excitation energy the emission of intermediate mass fragments (IMF, namely Z≥3) has been clearly observed [1, 2]. Experimentally one of the major difficulties concerns the precise characterization, in size and excitation energy, of the nucleus which undergoes the multifragment deexcitation. Consequently a good understanding of the reaction mechanisms involved in these collisions is required. It is now well established that the intermediate energy regime is characterized by the dominance of quasi-binary dissipative interactions in which a quasi-projectile and a quasi-target emerge from the collisions with an excitation energy which increases as the impact parameter decreases. However, in contrast with deep inelastic collisions at low energy (≈ 10 MeV/nucleon), the zone of overlap between projectile and target is subjected to a strong emission of particles and fragments (mid-rapidity emission) which blurs the purely binary scenario [3]. Nevertheless, the essentially binary nature of the collisions permits to produce well characterized projectile-like (QP) and target-like (QT) nuclei over a broad range of excitation energies which may reach and even exceed the available center of mass energy. Only at incident energy below ≈ 50 AMeV an incomplete fusion process can be observed in the most central collisions.

In this contribution we will present the method used to reconstruct the QP and the QT nuclei following the binary ^{36}Ar+^{58}Ni collisions up to 95 AMeV incident energy and show the various decay modes of these nuclei as a function of excitation energy, from standard evaporation to full vaporization in passing through the multifragmentation regime.

II Experimental method

The 4π detection array INDRA at GANIL was used to investigate the reaction ^{36}Ar+^{58}Ni at 32, 40, 52, 63, 74, 84 and 95 MeV/nucleon. A detailed description of INDRA, an ensemble of 336 telescopes covering 90% of the 4π solid angle, can be found in references [4, 5, 6]. For fragments with Z>3, charge identification is made up to Z≈50, down to an energy threshold of ≈1 AMeV for Z≈6 and ≈1.7 AMeV for Z≈50. For elements with Z≤3 isotopic separation is also achieved.

Beams of ^{36}Ar produced by the GANIL facility were used to bombard a 193 μg/cm^2 thick self-supporting ^{58}Ni target. In order to maintain the probability for multiple interactions in the target below 10^{-4}, the beam intensity was kept around 3-4$\times 10^7$ pps. Data were taken using a minimum bias trigger based on the multiplicity M such that events were registered for M≥3 for bombarding energies up to 74 AMeV and M≥4 above.

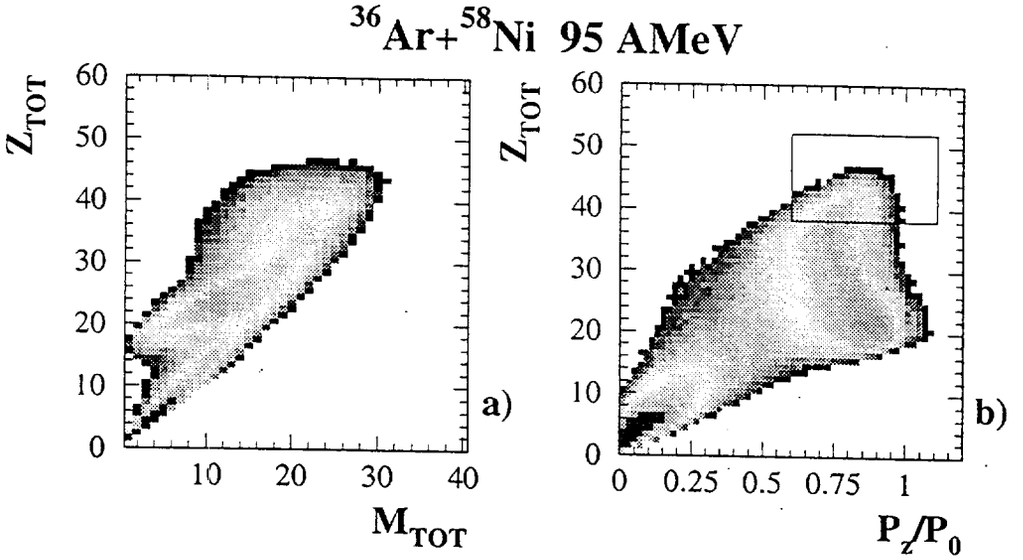

FIGURE 1: *Total detected charge as a function of the total charged particle multiplicity (a) and of the fraction of the beam momentum detected along the beam axis (b) at 95 AMeV bombarding energy for the Ar+Ni reaction. Selected quasi-complete events are indicated by the rectangle.*

In Fig. 1, the total detected charge, Z_{tot}, is presented as a function of the total multiplicity M_{tot} of the detected charged particles and fragments and of the total measured momentum along the beam direction P_z relative to the beam momentum, P_0, at 95 AMeV incident energy. Three regions are visible on these diagrams. For $Z_{tot} < 18$ and $P_z/P_0 < 0.5$, neither the quasi-projectile nor the quasi-target have been detected. This corresponds to the most peripheral collisions in which the projectile is scattered at angles smaller than 2° and the recoiling target does not have enough energy to overcome the detector thresholds. For $18 < Z_{tot} < 28$ and $P_z/P_0 > 0.6$, the quasi-projectile is detected but the quasi-target is still too low in energy. Finally, for $Z_{tot} > 28$, and $P_z/P_0 > 0.6$, both the QP and the QT are observed. In this latter region the missing charge can be imputed to the detector efficiency (geometrical cover and detection thresholds). Besides the above mentioned effects, obviously, non detected neutrons contribute also to the missing momentum.

In the following we will consider only quasi-complete events in which more than 80% of the total charge (46) of the system and more than 60% of the incoming beam momentum have been detected, as indicated by the rectangle in Fig. 1-b. These requirements eliminate mainly low multiplicity events (Fig. 1-a) corresponding to the most peripheral collisions.

As a measure of the violence of the collisions, we use the transverse kinetic energy, E_{tr}, defined as:

$$E_{tr} = \sum_i E_i \sin^2 \theta_i$$

where for a given event, the sum runs over all detected charged particles and where

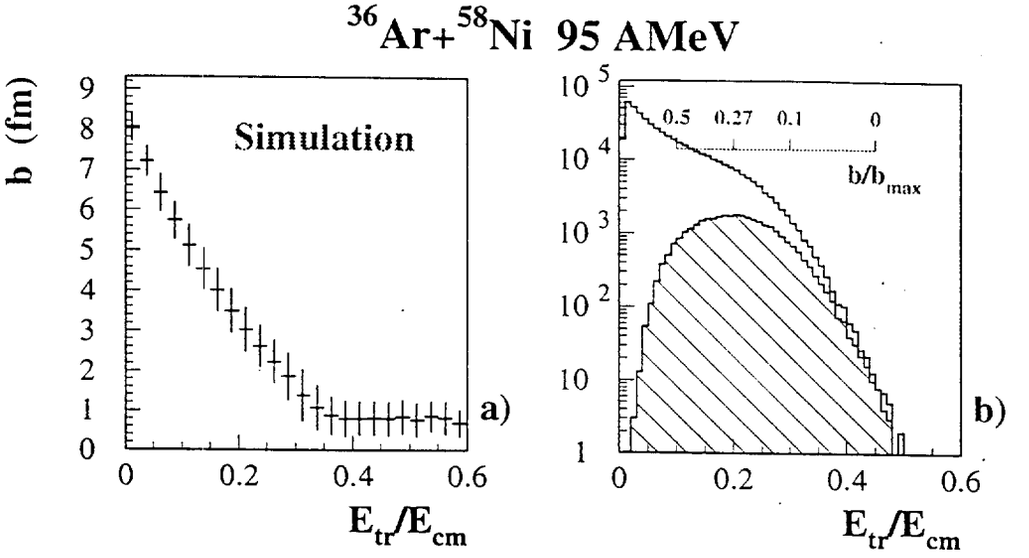

FIGURE 2: *a) Correlation between the transverse energy E_{tr}/E_{cm} and the impact parameter b predicted by a calculation based on a binary scenario in the 95 AMeV $^{36}Ar+^{58}Ni$. b) Measured E_{tr}/E_{cm} distributions corresponding to all detected events (full curve) and events analysed in this work (hatched histogram).*

E_i and θ_i are respectively the kinetic energy and emission angle of particle i.

Fig. 2-a shows the strong correlation between E_{tr}/E_{cm}, where E_{cm} is the available energy in the center of mass for the ^{36}Ar+^{58}Ni collisions at 95 AMeV, and the impact parameter b. This correlation is the result of a simulation of inelastic binary collisions followed by sequential deexcitation of both partners [7]. The larger E_{tr}, the more violent is the collision. The simulation leads to a fusion process below 1.5 fm. Fig. 2-b shows the transverse energy distributions for all events and for complete events (hatched area) in the 95 AMeV ^{36}Ar+^{58}Ni reaction. Assuming that the reaction cross-section $\sigma_R(b)$ up to an impact parameter b is essentially geometrical, $\sigma_R(b) = \pi\ b^2$, an estimate of the impact parameter can be obtained from the transverse energy through the relation:

$$\frac{b}{b_{max}} = \sqrt{\frac{1}{Y_{tot}} \int_{E_{tr}}^{E_{max}} \frac{dY}{dE_{tr}} dE_{tr}}$$

where $b_{max} \approx 9.6$ fm is the grazing impact parameter, Y_{tot} is the total measured yield whereas the integral represents the yield between the transverse energy E_{tr} and the maximum transverse energy E_{max}. The impact parameter scale reported inside Fig. 2-b shows that our selection of events mainly corresponds to collisions with: $0 \leq b \leq b_{max}/2$, including totally the most central ones: $b \leq 1$ fm.

In Fig. 3 are presented the charge distributions of the fragments with $Z \geq 3$ (IMF) as a function of their parallel velocity along the beam direction at 32, 52 and 95 AMeV bombarding energies for four transverse energy or impact parameter bins (see upper panel in Fig. 3). At all bombarding energies, from 32 AMeV to

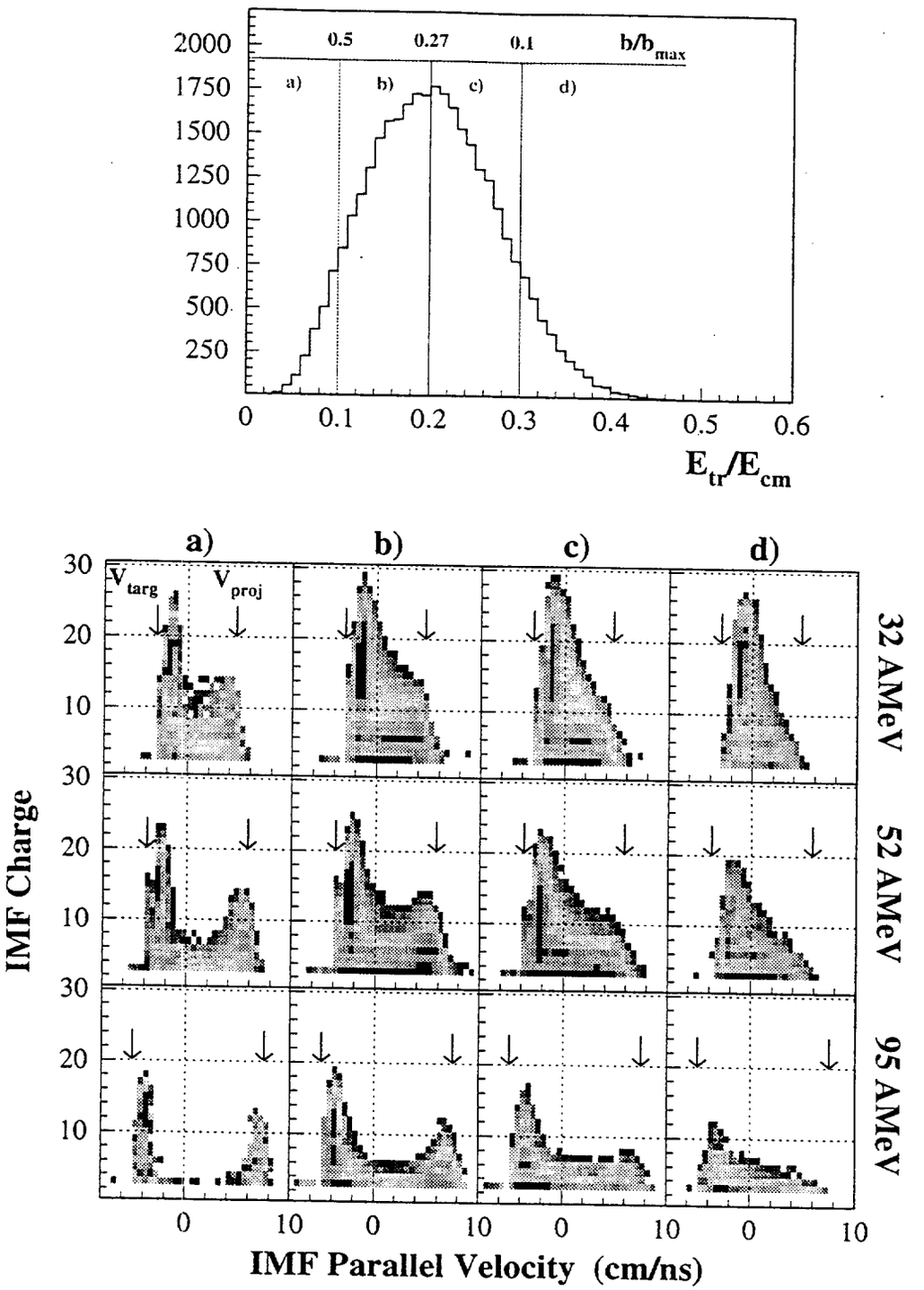

FIGURE 3: *Charge distributions of the fragments with $Z \geq 3$ (IMF) as a function of their parallel velocity in the center of mass frame at 32, 52 and 95 AMeV bombarding energies, for four impact parameter ranges: a) $b/b_{max} > 0.5$, b) $0.27 < b/b_{max} < 0.5$, c) $0.1 < b/b_{max} < 0.27$ and d) $b/b_{max} < 0.1$. Arrows show the center of mass target and projectile velocities. The upper part of the figure shows the E_{tr}/E_{cm} distribution and the four cuts.*

95 AMeV, for small transverse energies $E_{tr}/E_{cm} \leq 0.2$, the fragments are essentially located at velocities near the projectile or target velocities (as indicated by the arrows in Fig. 3), emphasizing the binary character of these collisions. For the most central collisions ($E_{tr}/E_{cm} \geq 0.3$), at 32 AMeV incident energy, some heavy fragments are produced with a velocity close to the center of mass velocity, suggesting an incomplete fusion process which seems to disappear around 52 AMeV and at 95 AMeV the binary character of the collision is clearly present (Fig. 3). However, at all impact parameters, the presence of fragments at mid-velocity may indicate some deviations from a purely binary process with an emission from the overlapping zone between projectile and target.

III Reconstruction of the primary sources

Before studying the deexcitation of the QP and the QT in the ^{36}Ar+^{58}Ni reaction it is necessary to reconstruct, from the kinematical properties of the detected fragments and charged particles, the primary sources. This was done, event by event, using the "Minimum Spanning Tree" (MST) technique [8], which consists in finding the minimum path linking N points in a metric space. For the present analysis [9], the method was applied in the velocity space where the "distance" d_{ij} between two particles is defined as the square of their relative velocity β_{ij}:

$$d_{ij} = \beta_{ij}^2 = \frac{(\vec{\beta}_i - \vec{\beta}_j)^2 - (\vec{\beta}_i \times \vec{\beta}_j)^2}{1 - (\vec{\beta}_i \vec{\beta}_j)^2}$$

where $\vec{\beta}_i$,$\vec{\beta}_j$ are the velocities of particles i and j respectively. As the origin of Z=1 particles is not well defined, the minimum tree is built for Z$\geq$2 particles only. Then, the largest link which maximizes the thrust T_2 is broken to form two clusters. The thrust [10], T_2, is defined in the center of mass frame as follows:

$$T_2 = \frac{|\sum_{i \in C_1} \vec{p}_i| + |\sum_{j \in C_2} \vec{p}_j|}{\sum_{k \in C_1 \cup C_2} |\vec{p}_k|}$$

where $\vec{p}_i$,$\vec{p}_j$ are the momentum of Z$\geq$2 particles, i and j attributed to clusters C_1 or C_2 respectively. The distribution of the maximized T_2 is plotted in Fig. 4 for the ^{36}Ar+^{58}Ni reaction at 95 AMeV. The binary character of such a reaction has been shown, in the previous section and in reference [11], and obviously the T_2 distribution exhibits a maximum rather close to T_2=1 (for a single source the maximum should be peaked around 0.5). In fact for small value of T_2 the method could be spurious, arbitrarily creating two sources in an event although it results from the deexcitation of one single source. Thus to enhance the degree of confidence in the result of the method only events for which the value of T_2 is larger than 0.65 have been selected and considered as two source events. Hence around 10% of "complete" events rejected in the present analysis could be good candidates for a single source deexcitation.

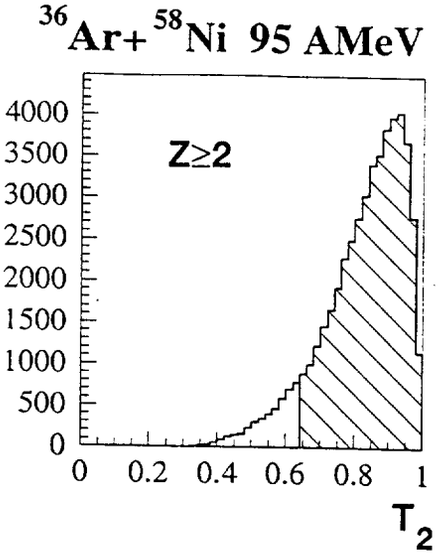

FIGURE 4: *Distribution of the thrust T_2 when the largest link which maximizes T_2 is broken to form two clusters in the 95 AMeV ^{36}Ar+^{58}Ni. The hatched area represents the selected events analysed as two source events (see text).*

Once this procedure is achieved, the hydrogen isotopes are distributed among the two clusters on proximity criteria. The properties of the emission sources thus obtained were tested against different reconstruction techniques [12, 13] which were found to yield essentially the same results. Taking into account the detection efficiency, the average charges and masses of the reconstructed quasi-projectile ($Z_{QP} \approx 15$) and quasi-target ($Z_{QT} \approx 25$) are very close to those of the initial projectile and target for the whole energy dissipation domain (Fig. 5-a). However the width of the distributions increases from $\approx 10\%$ to $\approx 20\%$ when going from peripheral to central collisions. It is now possible to study the properties of each source.

IV Energy sharing between QP and QT

The amount of excitation energy, E^*, imparted to the QP or to the QT is determined event by event by calorimetry through the relation:

$$E^* = \sum_{i=1}^{M_c} E_i + \sum_{j=1}^{M_n} \bar{K}n_j - Q$$

where M_c and M_n are the multiplicities of charged particles and of neutrons respectively. The value of M_n, which is not measured, is deduced from mass and isospin conservation, E_i are the kinetic energies of each particle (in the source reference frame). The average kinetic energy $\bar{K}n_j$ of the neutrons is taken as the average kinetic energy of the protons in the event minus 2 MeV to take into account the absence of Coulomb barrier. Finally, Q is just the mass balance. In

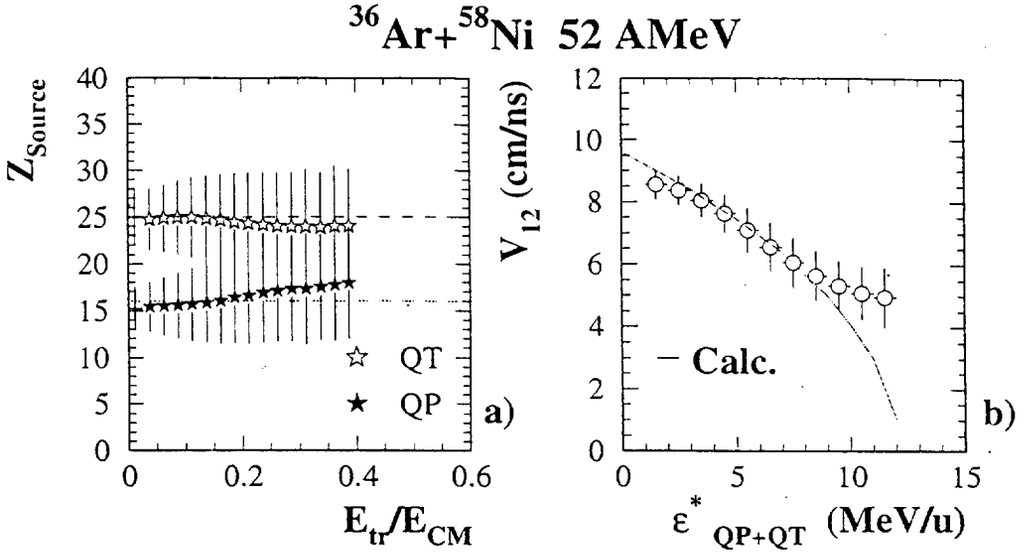

FIGURE 5: *a) Mean values of the charge distributions of the two reconstructed sources (QP and QT) as a function of the tranverse energy E_{tr}/E_{cm}. Error bars correspond to the width of the charge distributions. b) Correlation between the relative velocities V_{12} of the two sources and the total excitation per nucleon carried away by the QP and QT. The line reflects a kinematical calculation of the inelastic scattering 52 AMeV $^{36}Ar+^{58}Ni$ reaction.*

Fig. 5-b we compare the experimental correlation between the relative velocity V_{12} of the sources and the excitation energy per nucleon ϵ^*_{QP+QT}, taken away by the QP and QT, with a simple kinematical calculation assuming only an inelastic scattering in the ^{36}Ar+^{58}Ni reaction at 52 AMeV. The agreement is quite good, strengthening the hypothesis of binary reaction, except for large excitation energies $\epsilon^*_{QP+QT} > 9$ MeV/u where the relative velocities keep a constant value: $V_{12} \approx 4.5$ *cm/ns*. This is due to our method of reconstructing two sources: by using the thrust we maximize the relative velocity. In other words, we reach the limit of validity of the method.

Some features of the QP and QT in the ^{36}Ar+^{58}Ni reaction at 95 AMeV bombarding energy are shown in Fig. 6. The QP and QT mass distributions (Fig. 6-a), not corrected for detector efficiency, are relatively broad but remain peaked close to the masses of the projectile and target respectively. The average QT excitation energy is larger than that of the QP (Fig. 6-b), but (Fig. 6-c) the QP carries an amount of excitation energy per nucleon somewhat larger than the QT. Both QP and QT excitation energies per nucleon cover a broad range, extending from ≈4 MeV/u to ≈25 MeV/u and from ≈4 MeV/u to ≈20 MeV/u respectively.

In Fig. 6-d, the total excitation energy per nucleon imparted to the QP and QT is compared to the total energy, ϵ^*_{tot}, reconstructed in the center of mass of the system ^{36}Ar+^{58}Ni at 95 AMeV. For a perfect detection system, ϵ^*_{tot} should be equal to the c.m. available energy (22.3 AMeV). The width of the ϵ^*_{tot} spectrum

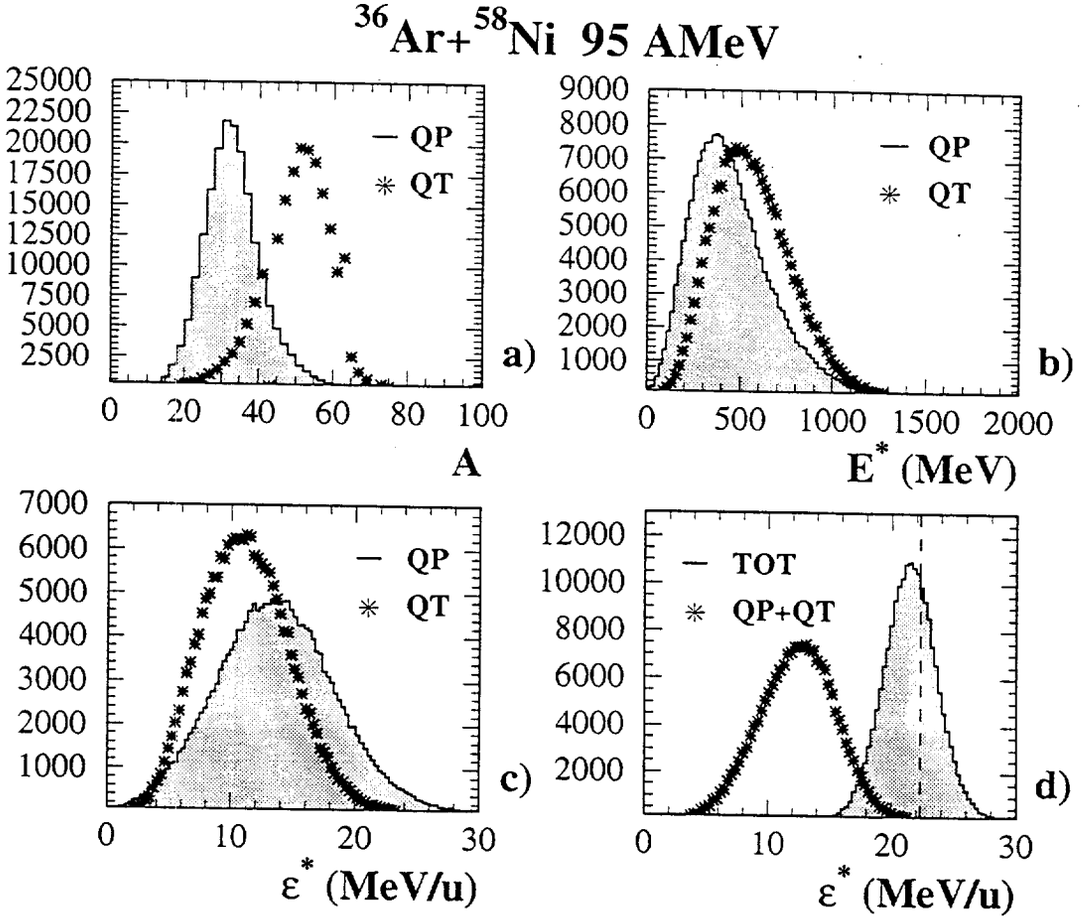

FIGURE 6: *Properties of the QP and QT deduced from quasi-complete events in the $^{36}Ar+^{58}Ni$ reaction at 95 AMeV bombarding energy a) Mass distributions of the QP and of the QT b) Excitation energy distributions in the QP and the QT c) Excitation energy per nucleon distributions in the QP and the QT d) Total excitation energy per nucleon distribution in the whole system (QP+QT) and total reconstructed energy (excitation energy + relative energy). The c.m. available energy is indicated by the vertical dashed line.*

can be considered as a measure of the overall precision of the method. The difference between the total energy, ϵ^*_{tot}, and the total excitation energy imparted to QP and QT, ϵ^*_{QP+QT}, is just the energy of relative motion between QP and QT.

In Fig. 7 the excitation energy per nucleon, ϵ^*_{QT} in the QT is plotted versus the excitation energy per nucleon ϵ^*_{QP} in the QP as a function of the violence of the collisions given by the transverse energy, E_{tr}/E_{cm}, for the reactions ^{36}Ar+^{58}Ni at 52, 74 and 95 AMeV bombarding energies. The straight solid line in Fig. 7 represents an equal temperature ($\epsilon^*_{QP} = \epsilon^*_{QT}$) and the dotted line an equal excitation energy ($E^*_{QP} = E^*_{QT}$) sharing between QP and QT. The experimental points lie between these two lines and show that $\epsilon^*_{QP} > \epsilon^*_{QT}$. For the sake of comparison, taking into account the evolution of the masses of the QP and of the QT respectively with the transverse energy (or impact parameter), equal sharing of the total excitation energy ($E^*_{QP} = E^*_{QT}$) is indicated by the dashed lines in Fig. 7. We can observe that the experimental points in the 8 to 15 MeV/u excitation energy domain are close to the dashed lines, indicating a different temperature in the QP and the QT. For $\epsilon^*_{QP} > 15$ MeV/u we reach large excitation energy and the method to reconstruct the QP and QT has to be precisely checked. For low excitation energies the energy thresholds of the detectors may introduce some bias. We checked all these points through intensive simulations by using the event generator of D. Durand [7]. The code allows to choose the excitation energy sharing between the QP and QT: equal temperature ($T_{QP} = T_{QT}$ or $\epsilon^*_{QP} = \epsilon^*_{QT}$) or equal excitation energy ($E^*_{QP} = E^*_{QT}$). The events generated can be filtered by the acceptance of the INDRA detector.

The results of the simulations are shown in Fig. 8. Firstly let's look at unfiltered data (open symbols). If the starting hypothesis is equal temperature (full line), respectively equal energy sharing (dashed line), after the reconstruction of the QP and QT the correlations $T_{QP} = T_{QT}$, respectively $E^*_{QP} = E^*_{QT}$ are conserved except for the highest excitation energies where some slight deviations relative to the input hypothesis can be observed. They have to be interpreted as the limitation of our reconstruction method for the most dissipative collisions. But in the case of the filtered data the deviations are clearly seen for low excitation energies where the energy thresholds of INDRA play a major role. Indeed after filtering no data point lies below $\epsilon^*_{QP} < 4$ MeV/u. Obviously the energy thresholds bias the slowest nucleus, the quasi-target, coming from more peripheral collisions and exclude experimental data points in the low excitation energy domain (see Fig. 7). As a consequence correlations with $\epsilon^*_{QP} < 7$ MeV/u and $\epsilon^*_{QT} < 7$ MeV/u are poorly significant. However the simulation shows that our reconstruction method is able to distinguish between the two excitation energy sharing hypotheses and strengthens the experimental result indicating that no thermal equilibrium between the QP and QT is reached in the $8 < \epsilon^*_{QP} < 15$ MeV/u excitation energy range, suggesting that the thermalization time is greater than the interaction time t_{int}. The latter has been estimated at ≈ 40 fm/c at 95 AMeV to ≈ 70 fm/c at 52 AMeV for the ^{36}Ar+^{58}Ni reaction.

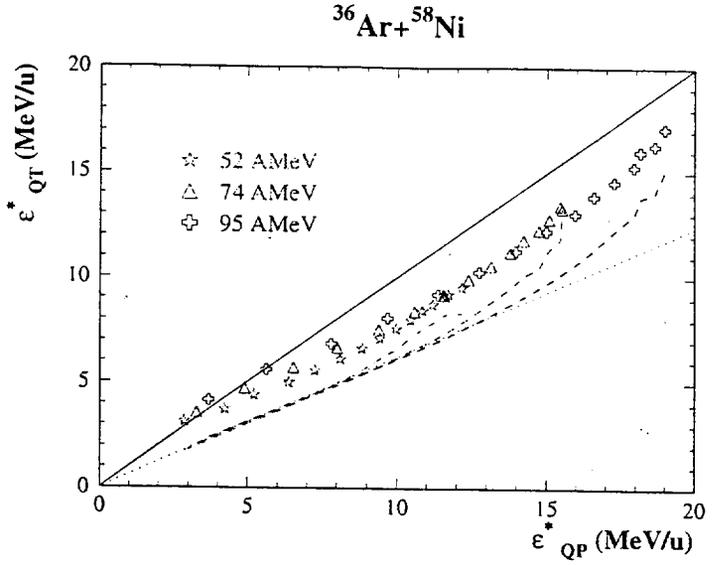

FIGURE 7: *Sharing of the excitation energy between the QP and QT as a function of the violence of the collision in $^{36}Ar+^{58}Ni$ at 52, 74 and 95 AMeV. The full and dotted lines correspond to equal temperature and equal excitation energy sharing, respectively, in QP and QT. The dashed lines are discussed in the text.*

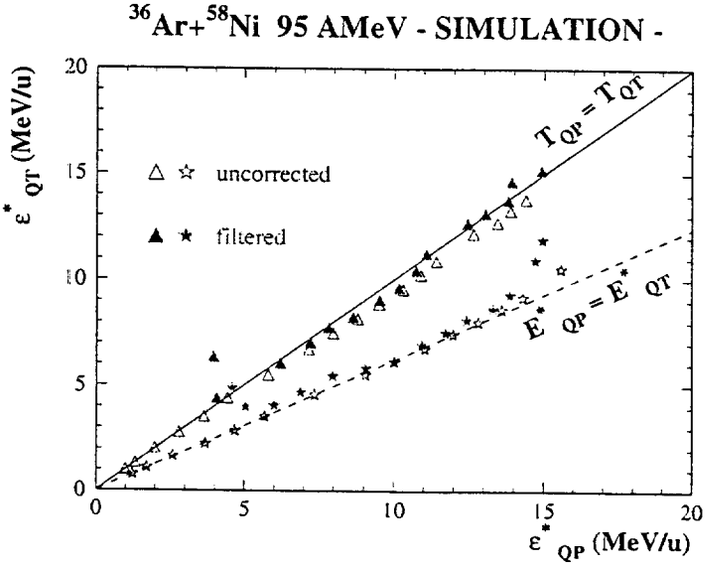

FIGURE 8: *Sharing of the excitation energy between the QP and QT as a function of the violence of the collision in a calculation simulating the binary reaction $^{36}Ar+^{58}Ni$ at 95 AMeV for two hypothesis: equal temperature (triangles) and equal excitation energy sharing (stars) in the QP and QT. Black symbols concern results filtered by the INDRA acceptance, open ones are unfiltered data.*

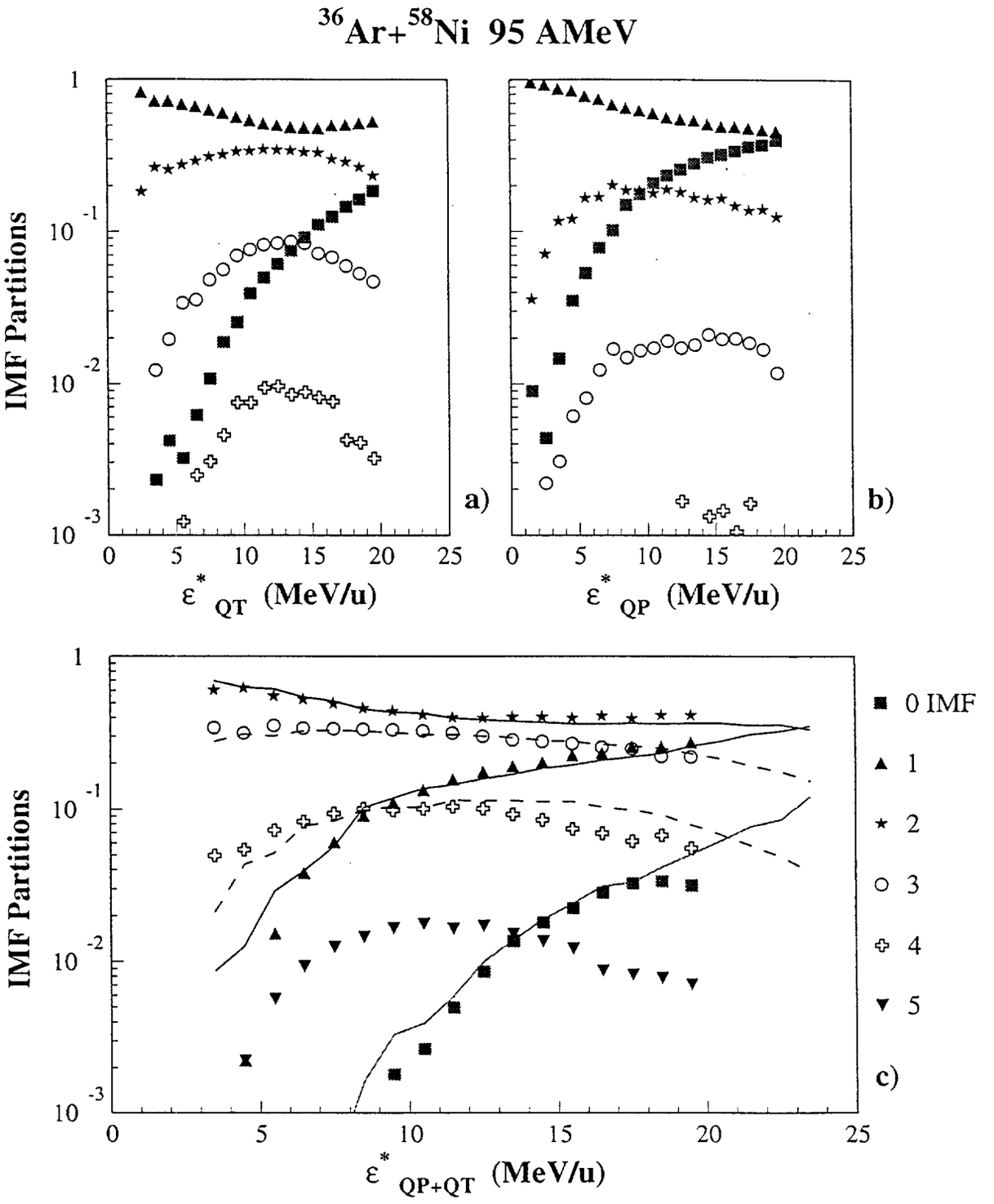

FIGURE 9: *Decay modes of the QT(a), the QP(b) and the whole system(c) as a function of the excitation energy in the reaction $^{36}Ar+^{58}Ni$ at 95 AMeV incident energy. Lines are results of a calculation presented in the text.*

V Decay modes and multi-fragment partitions

Fig. 9 depicts the decay modes of the QP, the QT and the whole system as a function of the excitation energy per nucleon, respectively: ϵ^*_{QP}, ϵ^*_{QT} and ϵ^*_{QP+QT} in the reaction ^{36}Ar+^{58}Ni at 95 AMeV. For each excitation energy bin, are reported the probabilities $P_n(\epsilon^*)$ of n-fragment emission, with $0 < n < N$ where N is the maximum number of observed fragments. For a given ϵ^* the $P_n(\epsilon^*)$ add to one. Following the evolution of the multi-fragment partitions in the QP and QT in Fig. 9-a-b we can argue: at low excitation energies the QP and the QT decay mainly by light particle emission leaving only one residue. The 2-fragment partition (fission-like process) is about two times more probable for the QT than for the QP. Higher-order partitions, corresponding to multifragmentation, increase rapidly with excitation energy, reach a maximum around 10-13 MeV/u of excitation energy and then decrease. The most dramatic evolution is seen in the no-fragment partition which increases continuously with excitation energy to become the dominant decay mode of the QP at the highest excitation energies. This last decay mode corresponds to a complete disintegration into light particles (H and He isotopes) [14]. In other words this evolution can be seen as the "rise and fall" of the multifragmentation process [15] due here to finite size effects. Note that the energy threshold for vaporizing a quasi-argon (QP) or quasi-nickel (QT) is around 3-4 MeV/u.

The partitions of the whole system (QP+QT) as a function of the excitation energy ϵ^*_{QP+QT} are shown in Fig. 9-c. Obviously, the two-fragment partition is now predominant emphasizing the binary character of the reaction. For a given excitation energy ϵ^* in the total system, these partitions can be deduced from the partitions of the QP and of the QT at the corresponding excitation energies ϵ^*_{QP} and ϵ^*_{QT}, using the relation:

$$P_n^{tot}(\epsilon^*) = \sum_{i=0}^{n} P_i^{QP}(\epsilon^*_{QP}) P_{n-i}^{QT}(\epsilon^*_{QT})$$

where, P_n^{tot} , P_i^{QP} and P_{n-i}^{QT} are respectively the probabilities for partitioning the whole system into n fragments, the QP into i fragments and the QT into $n-i$ fragments. The partitions thus calculated for $0 < n < 4$, are indicated by the full curves in Fig. 9-c. The agreement with the data is excellent, indicating that the QP and the QT decay independently from one another. The fact that the vaporization decay mode is well reproduced by such a calculation strengthens the conclusion of other analyses of the same data, where binary dissipative collisions were found to be the dominant mechanism for the production of vaporization events [12]

VI Conclusion

The reaction ^{36}Ar+^{58}Ni has been studied in detail from 32 to 95 AMeV bombarding energy. Over this whole energy range, the reactions remain essentially

binary in nature even for the most central collisions except below 50 AMeV where some fusion may still occur. An original procedure, the minimum spanning tree method, has been developed, and checked by intensive simulations, to reconstruct the two primary sources issued from the reaction. No thermal equilibrium has been reached before the separation of the two partners pointing out a thermalization time longer than the interaction time. The decay modes of the quasi-projectile and quasi-target have been explored over a broad excitation energy range (up to 25 MeV/u). In such small systems like ^{36}Ar or ^{58}Ni the multifragmentation regime seems to set in at $\approx$ 5 MeV/u excitation energy. Firstly the multifragmentation probability increases with the excitation energy, then saturates and decreases whereas the vaporization decay mode becomes sizeable above 10 MeV/u excitation energy. Moreover the study of the multi-fragment partitions shows that the QP and the QT decay independently from one another, even for the most dissipative collisions.

References

[1] L.G. Moretto and G.J. Wozniak, Ann. Rev. Nucl. Part. Sci. 43 (1993) 379 and references therein.

[2] J.P. Bondorf et al. Phys. Reports 257 (1995), and references therein.

[3] J. Lukasik et al., Phys. Rev. C in press.

[4] J. Pouthas et al., Nucl. Inst. and Meth. A357(1995)418.

[5] J-C. Steckmeyer et al., Nucl. Inst. and Meth. A361(1995)472.

[6] J. Pouthas et al., Nucl. Inst. and Meth. A369(1995)222.

[7] D. Durand, Nucl. Phys. A541 (1992) 266.

[8] J.C. Gower and G.J.S. Ross, Appl. Statistics, 18(1969)54.

[9] L. Nalpas, Ph.D. thesis, Université de Paris XI,1996.

[10] J. Cugnon and D. L'Hote, Nucl. Phys. A397 (1983)519.

[11] R. Dayras et al., Proceeding of the 7^{th} French-Japanese Meeting (1996), Dogashima (Japan) - Rapport CEA/DAPNIA/SPhN 97-14

[12] M-F. Rivet et al, Phys. Lett. B388(1996)219.

[13] Y.G. Ma et al, Phys. Lett. B390(1997)41.

[14] Ch.O. Bacri et al, Phys. Lett. B353(1995)27.

[15] C.A. Ogilvie et al, Phys. Rev. Lett. 67(1991)1214.